RSC Advances

ROYAL SOCIETY OF CHEMISTRY

www.rsc.org/advances

Electronic Structure and Optical Properties of Ag-doped SnO_2 nanoribbon

Bao-Jun Huang, Feng Li, Chang-Wen Zhang, Ping Li, Pei-Ji Wang *

School of Physics, University of Jinan, Jinan 250022, People's Republic of China

Abstract: Structural, electronic and optical properties have been calculated for Tin dioxide nanoribbons (SnO_2 NRs) with both zigzag and armchair shaped edge by first principle spin polarized total energy calculation. We find that both zigzag and armchair SnO_2NR have indirect band gaps. The band gap oscillates between the maximum of 3.38eV and the minimum of 1.69eV and eventually levels off to a certain value of 2.09eV for armchair nanoribbons, while for zigzag nanoribbons, the band gap oscillates between the maximum of 2.25eV to the minimum of 2.04eV and eventually levels off to 2.18eV. Our investigation further reveals that the optical absorption capacity enhanced with increasing the ribbon width for both Z-SnO_2NRs and A-SnO_2NRs. More interesting, when introducing Ag impurities, the optical absorption edge shift to low energy region. These findings can be a useful tool for the design of new generation of materials with improved solar radiation absorption.

Key words: Tin dioxide; nanoribbons; Ag-doped; electronic structure; optical properties.

*Corresponding author: School of Physics, University of Jinan, Jinan 250022, China

Tel: +86 531 82765965. E-mail adress: ss_wangpj@ujn.edu.cn （Pei-ji Wang）

1. Introduction

One-dimensional (1D) nanomaterials, such as nanowires, nanotubes, and nanoribbon, have been the subject of intensive research during the past two decades, because of the fundamental scientific interest in nanoscale-confined systems as well as the intriguing properties that are expected to be imporant for future nanodevices.[1] Recently, graphene nanoribbons(GNRs), Which are geometrically terminated single graphite layers, have gained considerable attention[2-9]. By applying transverse electric field to zigzag GNRs, half-metallicity can be achieved, rending them promising candidate materials for spintronic devices [2,6]. The electronic and optical properties of GNRs can also be modulated by changing both family and edge termination [10]. In addition, experimental realization of GNRs with various width and crystallographic orientations is more facilitative and flexible than carbon nanotubes(CNTs), through standard lithographic procedures or chemical methods[5,7].

Inspired by the unique properties of GNRs, much effort has been paid in find nanoribbons of other materials, such as boron nitride (BNNRs) [11,12], molybdenum disulfide (MoS_2NRs)[13,14], silicon (SiNRs)[15], and zinc oxide (ZnONRs) [16,17]. The single-layer materials of these materials are semiconducting with wide band gaps, in contrast to zero-band gap graphene. However, spin-polarization of the edge states and the value of band gaps have been predicated for these nanoribbons, which is sensitive to edge termination and ribbon width. Recently, Titanium oxide nanoribbons (TiO_2NRs) have also been predicted [18]. More interestingly, the electronic properties of such 2D materials could be modulated through some perturbative means, such as there has been recent work in using dipolar molecules that "break" the electronic symmetry of the 2D material and cause a dramatic change in the band gap[19], and molecular-logic quantum sensor where opto-mechanical stimuli are used as inputs and the spin-polarized current induced in the nanoribbon substrate is the measured output.[20] These works extend the applications of inorganic nanoribbons in nanoscaled devices.

Tin dioxide (SnO_2) is a versatile oxide semiconductor for its fascinating performance in fields ranging from photocatalyst[21.22], chemical gas sensor[23] dye-sensitized solar cells[24], and spintronic devices[25]. Considerable theoretical works have been devoted to the geometric and electric properties of SnO_2 nanometerials using first-principle[26,27]. Experimentally, two-dimensional (2D) ultrathin SnO_2 nanofilms and one-dimensional (1D) SnO_2 nanoribbon have been synthesized by thermal evaporation and post-processing [28,29].

It is rationally expected that the SnO_2 nanoribbons (SnO_2NRs) can be produced from ultrathin SnO_2 nanosheet (USnO_2NS), probably via the well established technique of fabricating GNRs from graphene. The orientation, edge structure and ribbon width of SnO_2NRs provides abounding freedoms to tune their electronic properties. In our previous work, we studied the electronic structure and optical properties of Ag-doped SnO_2 monolayer[30]. Here we report our first-principles study on the geometric construction, electronic structures, and optical properties of SnO_2NRs. We found that both armchair and zigzag SnO_2NRs are semiconductor with indirect gap, and perfect SnO_2NRs are spin-unpolarized wide-band gap semiconductors with variable band gap values depending on their growth orientation and width. Introducing Ag impurities can broaden the region of optical absorption for SnO_2NRs. Our work offers a promising route toward fabricating low-dimensional SnO_2 nanomaterials which have potential applications in solar cells and photoelectric sensors.

2. Methods and Computational Detalis

All the computations are performed with the spin-polarized first-principles methods as implemented in the Vienna ab initio simulation package(VASP),[31] to study on the electronic and optical properties of 1D SnO_2 nanostructures. Projector augmented wave (PAW) potentials and the Perdew-Burke-Ernzerhof[32] function under the spin-polarized generalized gardient correlation is used to describe the exchange and correlation interaction. The supercells are large enough to ensure that the vacuum space is at least 15A, so that the interaction between nanostructures and their periodic images can be safely avoided. Following the Monkhorst-Pack scheme[33], 12-k points were used for sampling the 1D Brillouin zone, and the convergence threshold was set as 10^{-4} eV in energy and 0.02eV/A in force. The valence electrons for the Sn, O and Ag are 14 （Sn: $4d^{10}5s^25p^2$), 6 (O: $2s^2$ $2p^4$) and 11($4d^{10}5s^1$). The positions of all the atoms in the supercell were fully relaxed during the geometry optimizations. On the basis of the equilibrium structures, 24-k points were then used to compute the electronic properties and 100-k points were used to compute the optical properties.

3. Results and discussion

3.1 Build model and band gap

The model structures of SnO_2NRs were generated by cutting an USnO_2NS along armchair and zigzag orientations, which are referred to as zigzag SnO_2 nanoribbons (ZSnO_2NRs) and armchair SnO_2 nanoribbons (ASnO_2NRs), as shown in figure 1. The SnO_2NRs with different widths are classified by the number of Sn lines (N_Z or N_A) across the ribbon width as shown in figure 1. After relaxation, the averaged Sn-O bond length in the center region of both 9-ASnO_2NRs and 9-ZSnO_2NRs are 2.11Å and 2.12 Å, whereas at the edges of 9-ASnO_2NRs and 9-ZSnO_2NRs shortens to 1.94 Å and 2.02 Å.The decrease of the bond length and the variation in the Coulomb forces at the nanoribbon edge may owing to the edge effect and slight out-of-plane structural distortion of zigzag and armchair segments along its width direction. Figure 1(c) and (d) presented the location of Ag-doped in armchair and zigzag nanoribbons.

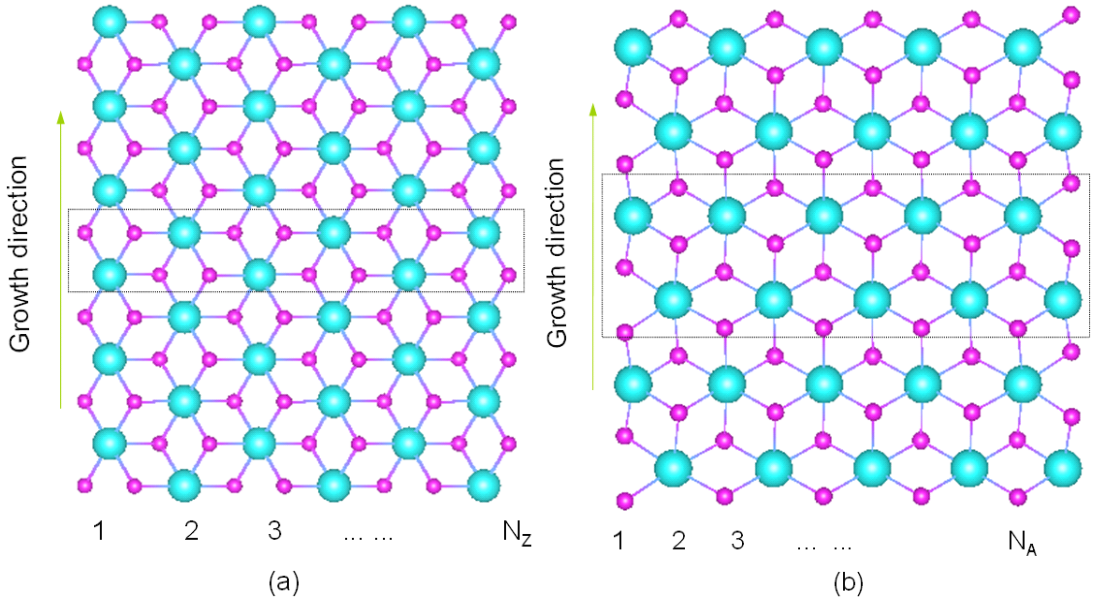

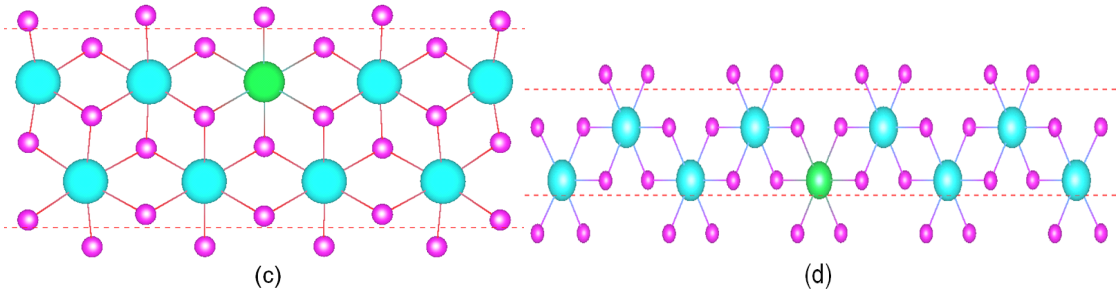

Figure 1. Top views of (a) $ZSnO_2NR$, (b) $ASnO_2NR$, (c)Ag-$ASnO_2NR$ and (d)Ag-$ZSnO_2NR$. The big cyan balls are Sn atoms, the small red balls are O atoms and the green balls are Ag atom. Grey dashed frameworks denote the unit cells. The variable Nz and N_A represent the numbers of Sn rows aligned perpendicularly to the $ZSnO_2NR$ and $ASnO_2NR$ growth direction, respectively.

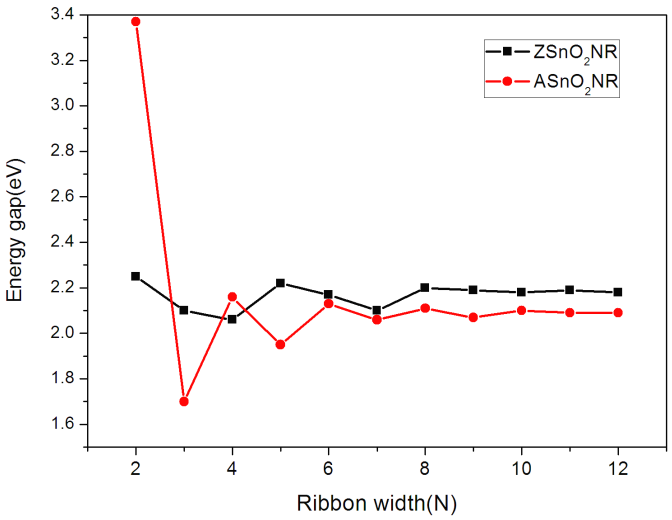

Figure 2. Energy gap evolution of $ZSnO_2NRs$ (black squares) and $ASnO_2NRs$ (red balls) as a function of ribbon width.

In order to study the variation of the band gap with ribbon width and directionality, the determined band gaps are plotted in figure 2 as a function of ribbon width N_Z for $ZSnO_2NRs$ and N_A for $ASnO_2NRs$ up to 12. It can be clearly seen that with increasing ribbon width and thus variation interaction between two edges, both band gaps of $ZSnO_2NRs$ and $ASnO_2NRs$ oscillate and final level off to a certain value 2.18eV for $ZSnO_2NRs$ and 2.09eV for $ASnO_2NRs$ respectively. This phenomenon is similar to TiO_2 nanoribbons[18]. Compared with the band gap of pure SnO_2 nanosheet (2.59eV) [30] which we calculated with generalized gradient approximation (GGA), there are 0.31 and 0.4eV decrement for $ZSnO_2NRs$ and $ASnO_2NRs$ respectively. The narrowed gap would consequently result in the electronic transition from Valence bands (VB) to conduct bands (CB) more easily. This would cause the absorption edge red shift to the longer wavelength region. It also resulted in a striking difference in the electro-hole pair formation.

3.2 band structure and density of electronic states

Figure 3 show the band structures and density of the electronic states (DOS) for 9-$ASnO_2NR$ and 9-$ZSnO_2NR$. We calculated the SnO_2 monolayer is a wide-gap semiconductor with a direct energy gap[30]. While from figure 3(a) and (b), we can seen that either $ASnO_2NR$ or $ZSnO_2NR$ have indirect band gaps, the lowest

conduction band (LCB) located at the Γ point and the highest valence band (HVB) located at the K point. This would be favorable to hinder the recombination of excited electron-hole pairs because of the difference of momentum between the two positions in the k-space[35]. The electronic states of HVB arise from the 2p states of O atoms and LCB almost originates from the 5p states of Sn atoms. Overall, both the narrow energy gap and indirect band gap could dramatically enhance the photocatalytic performance.

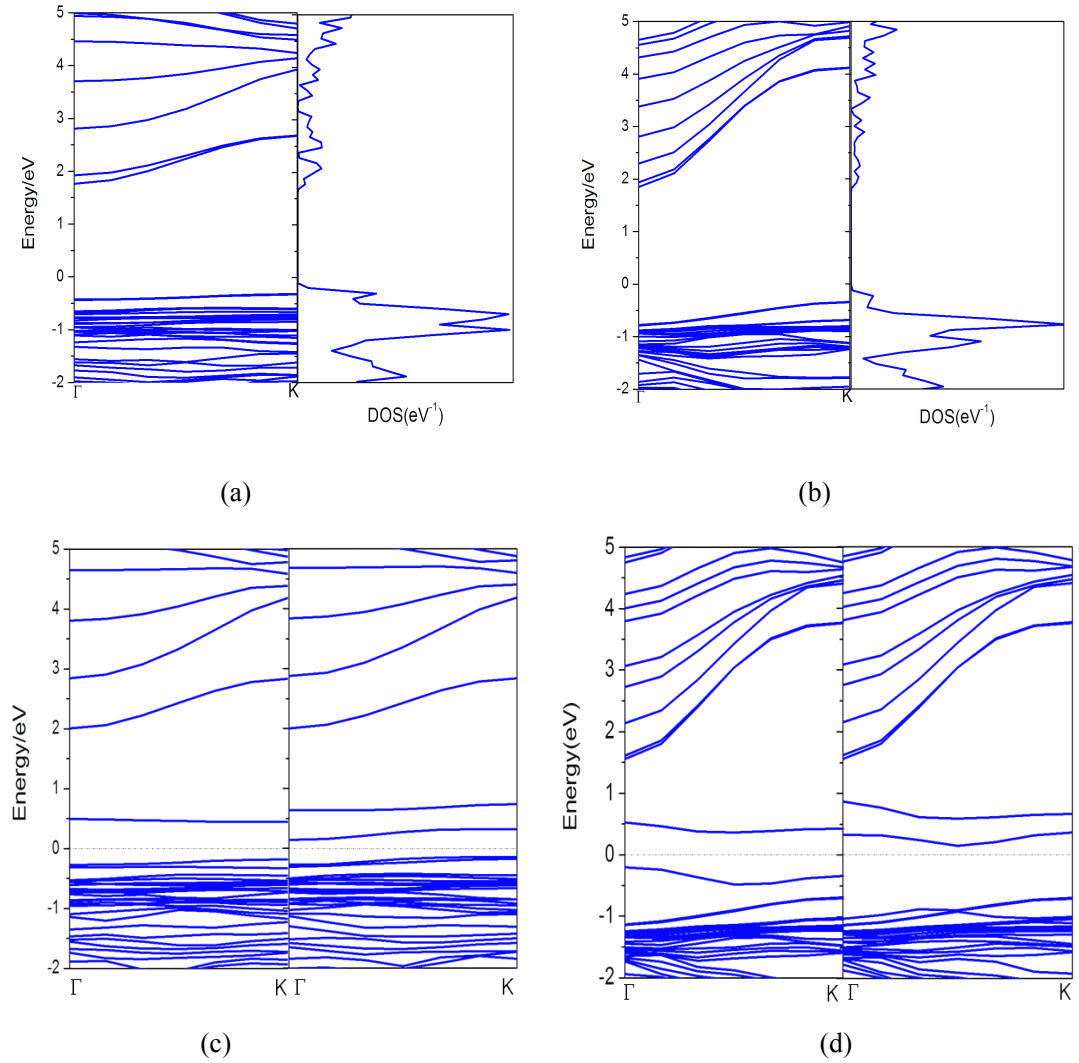

Figure 3. Band structure and density of states for 9-ASnO$_2$NR (a), 9-ZSnO$_2$NR (b) and spin band structure for Ag-doped 9-ASnO$_2$NR (c) and 9-ZSnO$_2$NR (d). The energy at the Fermi level (E_F) is set to zero.

The spin band structure of Ag-doped ASnO$_2$NR ZSnO$_2$NR are shown in figure 3(c) and (d), the calculations indicated that both ASnO$_2$NR and ZSnO$_2$NRs are semiconductor when introducing Ag impurities. Compared with the intrinsic SnO$_2$ nanoribbons, the band structure of Ag- doped SnO$_2$nanoribbon becomes more complicated. The Fermi level for ZSnO$_2$NR shift up instead of located at the valence band maximum by means of Ag doping, and the band gap narrowed due to the creation of impurity states in both valence and conduction band. Due to the doping of Ag in SnO$_2$ nanoribbon structure , there are some non-filled impurity energy levels in the neighborhood of Fermi level, and these impurity energy levels mainly originate from the 4d orbital electrons of Ag. The emergence of these energy levels would lead to the electronic intra-band or inter-band transition from the occupied

bands to the unoccupied ones under irradiation. This may induce intense absorption in the long wavelength visible region and infrared region.

To clearly analyze the influence of electronic structures and optical properties for metal-doped SnO_2NRS, The total density of states (TDOS) and partial density of states (PDOS) of the doped system were calculated and are shown in figure 4. The calculated energy gap (Eg) of Ag-doped SnO_2NRs were much less than that of pure

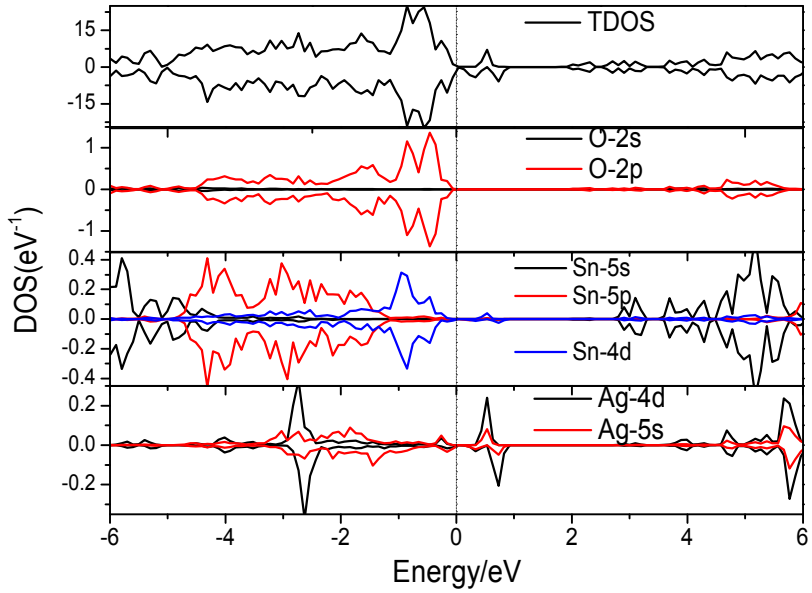

(a)

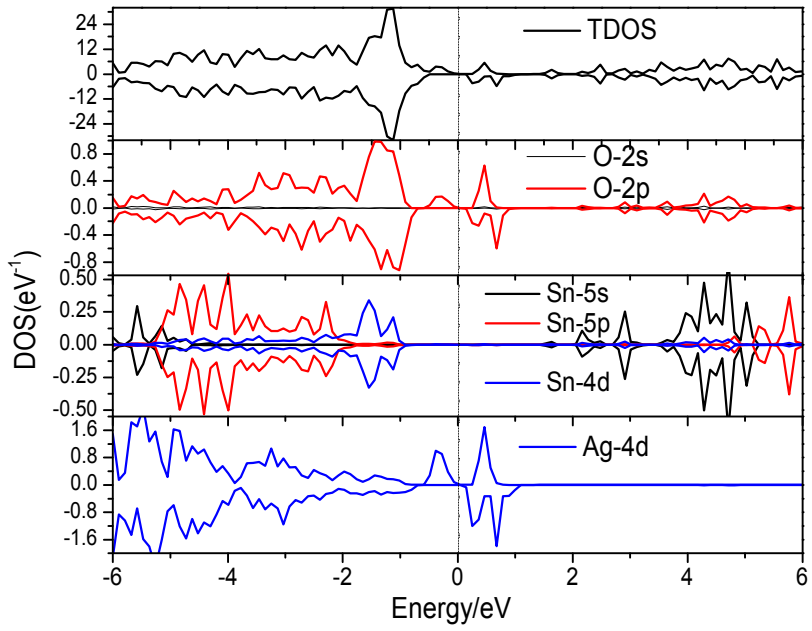

(b)

Figure 4. TDOS and PDOS of O, Sn and Ag atoms for (a) Ag-doped ASnO_2NRS and (b) Ag-doped ZSnO_2NRs.

SnO_2NRs because introducing Ag impurities, which consequently resulted in the electronic transition from VB to CB in Ag-doped SnO_2NRs more easily than that in pure SnO_2NRs. This would cause the absorption edge red shift to the longer wavelength region. It also resulted in a striking difference in the electron-hole pair formation. The

separation of electron and hole in Ag-doped models occurred more easily than that of intrinsic SnO_2NRs. We conclusion also showed Ag-doped SnO_2NRs are indirect-gap semiconductor, which would be favorable to hinder the recombination of the excited electron-hole pairs because of momentum between the two positions in the k-space[34.35]. Overall, both the narrow energy gap and indirect band gap could dramatically enhance the photocatalytic performance. As shown in figure 4(a), the lower VB between and -6.0 and -4.8eV were predominantly composed of Sn 5s orbital. The VB between -4.8 and -1.0eV mainly consisted of O 2p, Sn 5p and Ag 4d states, slightly hybridized with Ag 5s and Ag 4d states. The bands located in VB near the Fermi level mainly arise from O 2p orbital. The impurity bands located in CB near the Fermi level mainly arise from Ag 4d states and the internal hybridized between Ag 4d and 5s orbitals.The upper CB were predominantly composed of O 2p and Sn 5s states. From the above, when introducing Ag impurities, because of only one electron at outmost layer for Ag atom, the Ag-doped SnO_2NRs showed the P-semiconductor properties. Increased concentrate of holes enhanced the conductivity and promoted the improvement of photocatalytic efficient.

3.3 Optical properties

To examine the effect of Ag dopant on photocatalytic efficiency of the SnO_2NRs, the calculated optical absorption spectra of armchair (a) and zigzag (b) are presented in figure 5. The optical absorption property of a semiconductor materials was related to its electronic band structure as grapheme nanoribbon[36], which was a key factor in determining its photocatalytic activity. For pure SnO_2 monolayer and nanoribbons, the large E_g restricted its application only to the narrow light-response range of ultraviolet. When introducing Ag impurities, the optical absorption-edge of both ASnO_2NRs and ASnO_2NRs shifted to a longer wavelength region, which was in good agreement with the band structure investigation in the above section. Furthermore, the absorption intensity of Ag-doped systems enhanced significantly in the low-energy region corresponding to visible and infrared light region. The remarkable enhanced of the absorption might attribute to the electron transition of Ag 4d due to introducing Ag impurities.

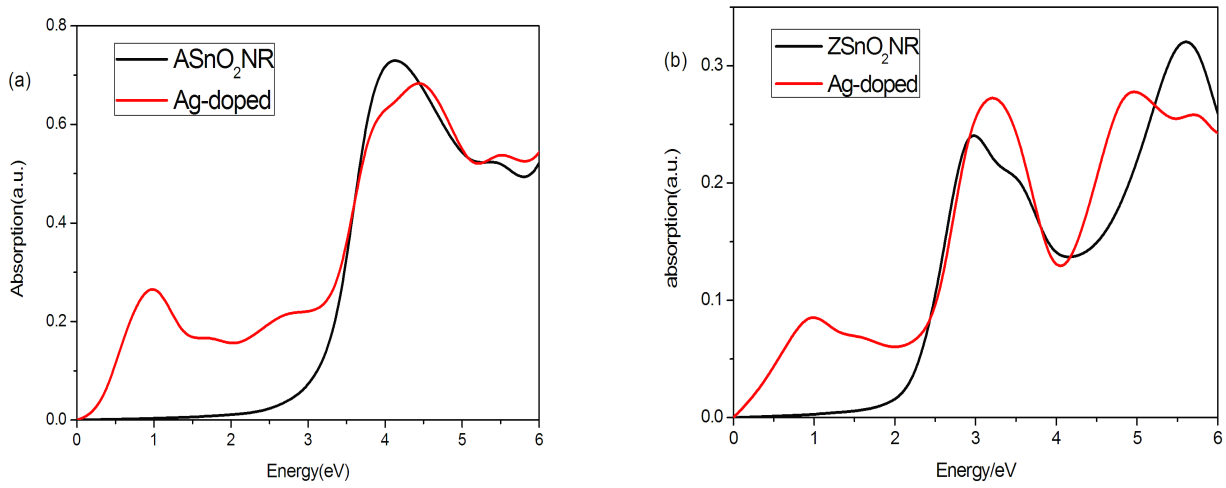

Figure 5. Calculated optical absorption spectra of armchair (a) and zigzag (b) SnO_2 nanoribbons.

Figure 6 shows the absorption spectra with the width of nanoribbons of n=2, 4, 6, 8, 10. For $ASnO_2NR$ of n=2, there are two obvious absorption peaks located at 4.4eV and 8.1eV, the other two lower peaks located at 6.3eV and 7.0eV. These peaks can be attributed to the combination of the transition between O 2p and Sn 5s and that between Sn 4d and Sn 5p. At the same time, there are some unapparent folded peaks, and they could be attributed to multi-levels direct or indirect transition. When the width of nanoribbons increases to n=4, 6, 8, and 10, the absorptive capacity have obvious enhance in the same wavelength range. Nevertheless, the absorption edge and peaks slight shift to low energy region, it can be explained that the band gap have not dramatic variation with increasing of the width of nanoribbons, as shown in figure 2. For $ZSnO_2NRs$, three obvious absorption peaks located at 3.6eV, 6.4eV and 9.1eV and the other two lower peaks located at 4.8eV and 8.4eV. When the width of nanoribbon increase to n=2, the absorption edge shift to low energy region dramatically, this is consistent with the variation of band gap. When band gap decrease, electrons can transition from valence band to conduct band more easily, in consequence, material have obvious absorption capacity in lower energy region. When the width of nanoribbons increases to n=4, 6, 8, and 10, the absorptive capacity have obvious enhance while the absorption edge almost no change. Have three intense absorption peaks located at 2.8~3.03V, 5.6~5.9eV and 8.4~8.7eV. These peaks derived from the transition between O 2p and Sn 5s and that between Sn 4d and Sn 5p similarly. The slight difference for the location of peaks can be attributed to the difference of band gaps.

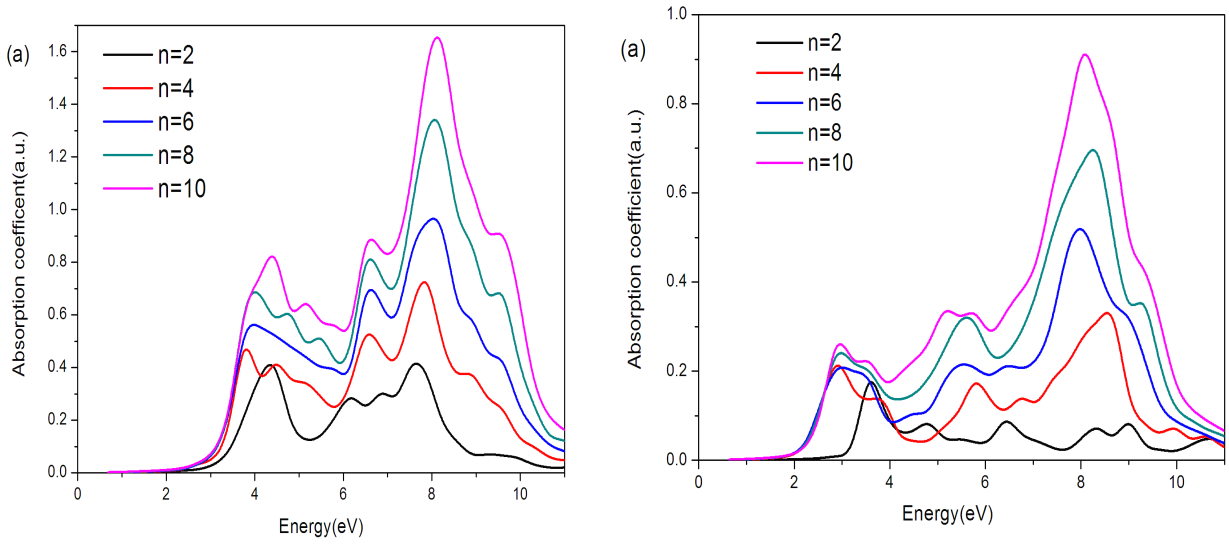

Figure 6. Optical absorption coefficient of $ZSnO_2NRS$(a) and $ASnO_2NRs$(b) with width variation

3.4 Binding energy

The stability of SnO_2NRs is also important because it can determine whether this nanostructure can be realized experimentally. To estimate the stability, we have computed the binding energy per atom for both zigzag and armchair nanoribbons as a function of the ribbon width. Here, the binding energy (E_b) is defined as $E_b=(\sum n_i E_i - E_{tot})/\sum n_i$, Where i represents different elements of Sn and O, n_i and E_i are the number and chemical potential for the corresponding element, respectively, and E_{tot} is the total free energy of system. The stability of different ribbon can be evaluated by the binding energy; those with larger binding energies are more stable according to the laws of thermodynamics.

As shown in figure 7, the binding energies of SnO_2 are lower than that of the SnO_2 monolayer (E_b=2.629eV) due to the quantum confinement, and they increase monotonically with the increasing ribbon widths for both zigzag and armchair SnO_2NRs except for 3-ASnO_2NR. The binding energies of zigzag ribbons are higher than those of armchair ones with comparable widths. This demonstrates vigorously that ZSnO_2NRs are energetically more favorable than ASnO_2NRs.

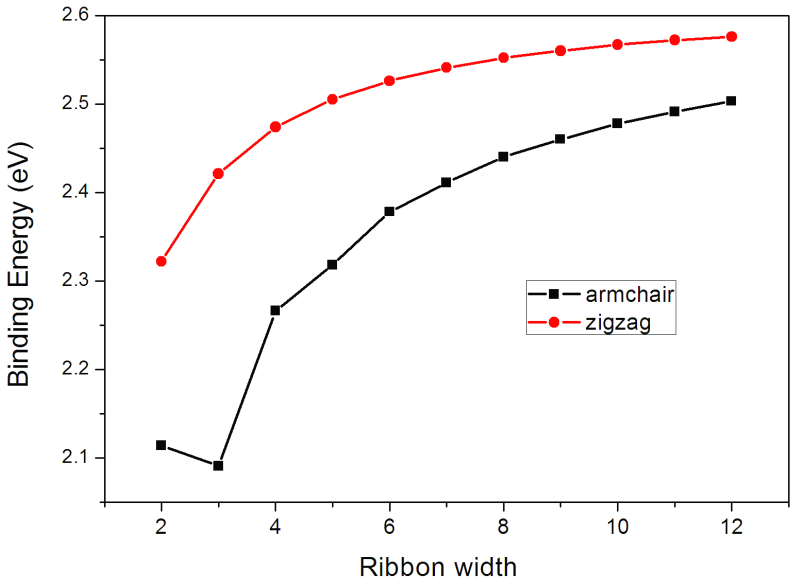

Figure 7. Binding energy per atom of ZSnO_2NRs and ASnO_2NRs as a function of the ribbon width.

4. Conclusion

In summary, first-principles calculations based on DFT were performed to understand the mechanisms of SnO_2NRs. The calculated conclusion shows that SnO_2NRs can be formed from the already-synthesized SnO_2 nanosheet along different edges. Both zigzag and armchair SnO_2NRs are indirect gap semiconductors with a band gap larger than 1.7eV. The band gaps of both ZSnO_2NR and ASnO_2NR as a function of ribbon width are zigzag and finally tend to a certain value respectively. With the introducing of Ag impurities, there are obvious red shift for the optical absorption edge and enhance absorption intensity in the low-energy region, which illustrated the enhanced mechanism of photocatalytic performance. With the variation of the width of nanoribbons, the absorption edge and capacity changed accordingly. These conclusions imply SnO_2NRs have potential applications in solar cells, photoelectronic devices and photocatalysts.

Acknowledge: This work was supported by the National Natural Science Foundation of China (Grant No. 61172028 11274143, and 11304121), the Natural Science Foundation of Shandong Province (Grant No. ZR2010EL017)

References

[1] Xia Y, Yang P, Sun Y, Wu Y, Mayers B, Gates B, Yin Y, Kim F, and Yan H. Adv. Mater, 2003, 15(5): 353-389.

[2] Son Y, Cohen M L, Louie S G. Nature. 2006, 444(7117): 347-349.

[3] Son Y W, Cohen M L, Louie S G. Phys. Rev. Lett. 2006, 97: 216803.

[4] Ezawa M. Phys. ReV. B 2006, 73: 045432.

[5] Li X L, Wang X R, Zhang L, Lee S W, Dai H J. Science 2008, 319(5867): 1229-1232.

[6] Kan E J, Li Z, Yang J L, Hou J G. Appl. Phys. Lett., 2007, 91(24): 243116.

[7] Yan Q M, Huang B, Yu J, Zheng F W, Zang J, Wu J, Gu B L, Liu F, Duan W H, Nano Lett., 2007, 7: 1469.

[8] Koskinen P, Malola S, Hakkinen H. Phys. ReV. Lett., 2008, 101: 115502.

[9] Lakshmi S, Roche S, Cuniberti G. Phys. ReV. B, 2009, 80: 193404

[10] Prezzi D, Varsano D, Ruili A, Marini A, and Molinari E. Phys. Rev. B, 2008, 77: 041404.

[11] Ding Y, Wang Y, Ni J. Appl. Phys. Lett., 2009, 94(23): 233107.

[12] Chen W, Li Y F, Yu G T, Li C Z, Zhang S B, Zhou Z, Chen Z F. J. Am. Chem. Soc, 2010, 132:1699.

[13] Li Y, Zhou Z, Zhang S, Chen Z. J. Am. Chem. Soc, 2008, 130: 16739-16744.

[14] Pan H, Zhang Y W. Journal of Materials Chemistry, 2012, 22: 7280-7290.

[15] Zheng F B, Zhang C W, Yan S S and Li F. Journal of Materials Chemistry C, 2013, 1: 2735-2743.

[16]Yan H, Johnson J, Law M, He R, Knutsen K, Mckinney J R, Pham J, Saykally R, Yang P. Adv Mater, 2003, 15(22): 1907-1913.

[17] Andrés B, Florentino L, Terrones M, Terrones, H. Nano Lett, 2008, 8(6): 1562-1565.

[18] He T, Pan F, Xi Z, Zhang X, Zhang H, Wang Z, Zhao M, Yan S, and Xia Y. J. Phys. Chem. C, 2010, 20(114): 9234-9238.

[19] Kim M, Safron N S, Huang C, Arnold M S, Gopalan P. Nano Lett, 2012, 12(1):182-187.

[20] Wong B M , Simon H Y, and O'Bryan G. Nanoscale, 2012, 4: 1321-1327.

[21] Liu Z Y, Sun D D, Guo P, Leckie J O. Nano letters, 2007, 7(4): 1081-1085.

[22] Wang W W, Zhu Y J, Yang L X. Advanced Functional Materials, 2007, 17(1): 59-64.

[23] Kim H, Haensch A, Kim I, Barsan N, Weimar U, Lee J. Advanced Functional Materials, 2011, 21(23): 4456-4463.

[24] Snaith H J, Ducati C. Nano Lett, 2010, 10(4): 1259-1265.

[25] Borges P D, Scolfaro L M R, Alves H W, Silva E F and Assali L V C. Nanoscale Research Letters, 2012, 7: 540-545.

[26] Scanlon D O, Watson G W. Journal of Materials Chemistry, 2012, 22: 25236-25245.

[27] Schleife A, Varley J B, Fuchs F, Rödl C, Bechstedt F, Rinke P, Janotti A, and VandeWalle C G. Phys. Rev. B, 2013, 87:239901.

[28] Joy K, Lakshmy S S, Thimas P V. J Sol-Gel Sci Technol, 2012, 61:179-184.

[29] Chen H T, Xiong S J, Wu X L, Zhu J, and Shen J C. Nano Letters, 2009, 9(5): 1926-1930.

[30] Huang B J, Li F, Zhang C W, Li P, Wang P J. Journal of The Physics Society of Japan, 2014, 83: 66457.

[31] Kress G and Joubert D. Phys. Rev. B, 1999, 59: 1758.

[32] Perdew J P, Burke K, and Ernzerhof M. Phys. Rev. Lett, 1996, 77: 3865.

[33] Monkhorst H J and Pack J D. Phys. Rev. B, 1976, 12: 5188.

[34] zhang H, Liu L, Zhou Z. Phys. Chen. Chem. Phys, 2012, 14: 1286-1292.

[35] Gao H T, Li X H, Lv J, and Liu G. The Journal of Physical Chemistry C, 2013, 117(31): 16022-16027.

[36] Prezzi D, Varsano D, Ruini A, Molinari E.. Phys. Rev. B, 2011, 84: 041401